arXiv:1607.08553v1 [cond-mat.mes-hall] 28 Jul 2016

Effective dimensionality of the indirect interaction on the edges of MoS_2 triangular flakes

O Ávalos-Ovando[1], D Mastrogiuseppe[2], and S E Ulloa[1*]

[1] Department of Physics and Astronomy, and Nanoscale and Quantum Phenomena Institute, Ohio University, Athens, Ohio 45701–2979, USA

[2] Instituto de Física Rosario (CONICET), 2000 Rosario, Argentina

E-mail: ulloa@ohio.edu

Abstract. We study the Ruderman-Kittel-Kasuya-Yosida interaction between two magnetic impurities connected to the edges of zigzag-terminated transition-metal dichalcogenide triangular flakes. When the impurities lie on the edges of the flake, the effective exchange configuration is helical, showing a sizable noncollinear Dzyaloshinskii-Moriya interaction. We analyze the interaction decay exponent for doping levels inside the band gap of the infinite layer, corresponding to edge states for the flake. The exponents show a sub-2D behavior for different band fillings, with a decay that is slower than quadratic. Remarkably, the noncollinear component can feature positive exponents, signaling an interaction that grows with the impurity separation. This effect can be attributed to the presence of an envelope with a wavelength longer than the size of the flake.

1. Introduction

Layered transition-metal dichalcogenides (TMDs) [1, 2] have received great attention due to their unique electronic and optical properties. These materials can be exfoliated down to a stack of three atomic layers, in which one layer of transition metal atoms is sandwiched between two layers of chalcogen species. Each material (e.g. MoS_2, WS_2, among others) has different electronic structures and properties, such as strong photoluminescence, large spin-orbit coupling (SOC) [3–5], and either direct or indirect band gap depending on the number of layers [6]. These properties make TMDs very promising for applications and devices [7]. The combination of strong SOC and the presence of magnetic dopants could render these materials good candidates for spintronic applications [8]. Therefore, it is necessary to understand the interaction between the electronic degrees of freedom and localized magnetic moments.

Magnetic impurities can be intrinsic to the sample production process or can be introduced extrinsically into different materials. When a finite concentration of magnetic species is present in a metallic sample, they can interact effectively via the conduction electrons by a process known as Ruderman-Kittel-Kasuya-Yosida (RKKY) interaction [9–11]. This interaction is long ranged and oscillating. In conventional metals it decays as r^{-d}, where r is the distance between impurities and d is the dimensionality of the electron gas. The oscillating behavior can produce a tendency to ferromagnetic (FM) or antiferromagnetic (AFM) alignment of the magnetic moments, depending on the band filling. However, when the conduction bands have nonstandard features, the interaction can have peculiar features. For instance, in graphene, the interaction

is found to decay as r^{-3} at the Dirac point, but in doped or spin-polarized graphene it decays as r^{-2} [12], as in conventional 2D materials.

TMDs are, in general, semiconducting materials, but they can be doped with electrons and/or holes. This allows one to reach energy sectors in which the SOC has strong influence in the band structure. It is well known that SOC can introduce anisotropic interactions between magnetic moments [13], which can give rise to helical spin structures. In TMDs the band splitting is much larger near the valence band maximum (VBM) than close to the conduction band minimum (CBM), so the p-doped case is more attractive.

The RKKY interaction on infinite p-doped TMD layers has been studied in previous works, considering only the bands near the Brillouin zone corners K and K' [14, 15], and with the inclusion of the important valence band at the Γ point, whose maximum lies close in energy to the ones at K and K' [16]. Although analyzing the case of infinite layers is essential, the process of exfoliation often produces nanoscale samples –nanoflakes– with different shapes and boundaries [17, 18]. Finite samples often have richer properties than the bulk counterpart, with characteristics that depend on the shape and termination. For instance, MoS_2 zigzag nanoribbons exhibit unusual ferromagnetic properties [19–21], probably due to the presence of edge states [22]. Also special intrinsic magnetism arises in triangular MoS_2 films, which depends on the type of edge termination [23, 24]. TMD zigzag edges have also been proposed to host Majorana fermions [25, 26].

The RKKY interaction has been studied in graphene samples [27–29]. We analyzed the RKKY interaction in zigzag-terminated triangular TMD flakes (one of the most usual shapes [18]) in previous work [30]. It was shown that the interaction decays slowly as r^{-1} or even slower, depending on the doping level, due to highly localized states distributed along the edges.

Using an effective three-orbital tight-binding model [31], we present here a systematic study of the decay for such states. We study the interaction between two magnetic impurities in triangular TMD flakes. We focus our attention on doping levels lying inside the optical gap, capturing states that concentrate on the edges of the flake. We analyze the decay exponent of the impurity separation as the chemical potential sweeps the midgap states, for the different components of the spin-spin interaction. We find that the exponent signals sub-2D behavior, with values that depend strongly on the different midgap states. Interestingly, the noncollinear Dzyaloshinskii-Moriya (DM) component can feature positive exponent, corresponding to an increasing impurity interaction with distance. This behavior can be explained by the presence of a long wavelength modulation envelope.

2. Model and Approach

We consider triangular zigzag-terminated MoS_2 nanoflakes [18], with two magnetic moments (or impurities) hybridized to different lattice sites, as shown in Fig. 1. A suitable approximation is to describe the system by a triangular lattice of only Mo atoms (see Fig. 1) since, at low energies, only three Mo d-orbitals contribute, with almost no p-orbital weight from the chalcogens. The Hamiltonian is given by $H = H_{3\mathrm{O}-\mathrm{TB}} + H_{\mathrm{I}}$, where $H_{3\mathrm{O}-\mathrm{TB}}$ describes the triangular TMD lattice [31, 32] and H_{I} is the Hamiltonian for two magnetic impurities interacting with the conduction electrons of the host.

In the infinite 2D MoS_2 monolayer, the first Brillouin zone has two inequivalent K and K' points, with a sizable spin-splitting around the VBM due to the SOC [see Fig. 2(a)]. There is a direct band gap ($\sim$ 1.6 eV) between the VBM and the CBM at these two points, with definite spin-valley relation due to the absence of inversion symmetry in the unit cell. On the other hand, for finite systems the electronic spectrum is discrete (see Fig. 2(b) and inset), showing both bulk- and edge-like states. States from both the valence and conduction bands have been brought into the gap, signaling 1D-like extended states localized near the borders of the sample [22, 33]. The Hamiltonian for the magnetic impurities connected to specific

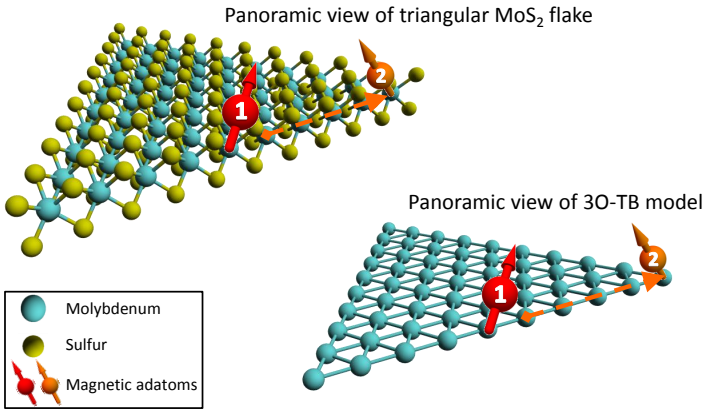

Figure 1. Views of the flake and tight-binding model, in which only three Mo d-orbitals are considered. Two magnetic impurities are connected to the edge of the flake, shown as red and orange arrows and labeled as 1 and 2. Impurity 1 is held fixed while impurity 2 moves along the zigzag edge, until the end of the flake, as shown by the dashed-orange trajectory.

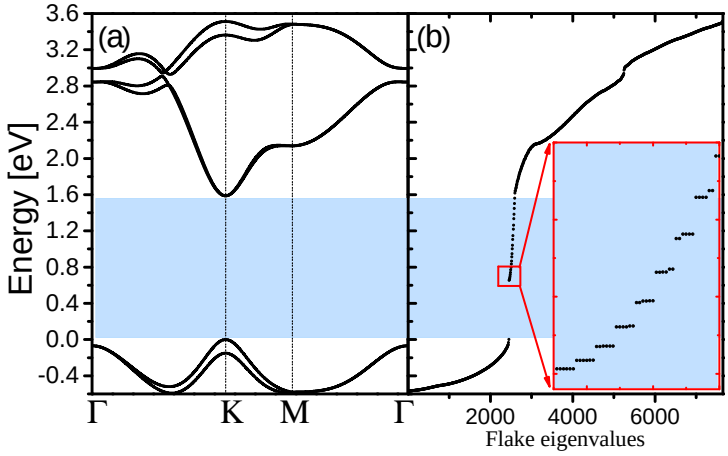

Figure 2. (a) Band structure for bulk MoS_2 monolayer obtained via the 3O-TB model. The gap is shown as a light blue area. The VBM at K is shifted to zero energy. (b) Discrete energy levels for a 50-row flake, showing midgap energy levels. Midgap state typical distribution is shown in the red inset, where one can see degeneracies due to spin and threefold symmetry.

sites of the TMD lattice is given by $H_{\rm I} = \mathcal{J}_\alpha \sum_{i=1,2} \mathbf{S}_i^{\rm imp} \cdot \mathbf{S}_\alpha(\mathbf{l}_i)$, where $\mathcal{J}_\alpha$ is the exchange coupling between the localized magnetic moment (either $i = 1, 2$) and the conduction electrons at lattice site $\mathbf{l}_i$ and orbital α (d_{z^2}, d_{xy} or $d_{x^2-y^2}$). $\mathbf{S}_i^{\rm imp}$ is the spin operator for the local magnetic moment i, and $\mathbf{S}_\alpha(\mathbf{l}_i)$ is the conduction electron spin operator at site $\mathbf{l}_i$ for orbital α. When $\mathcal{J}$ is small, the electronic degrees of freedom can be integrated out using second order perturbation theory in the bulk 2D crystal, yielding an effective exchange interaction of the form $H_{RKKY} = J_{XX}\left(S_1^x S_2^x + S_1^y S_2^y\right) + J_{ZZ} S_1^z S_2^z + J_{DM}\left(\mathbf{S}_1 \times \mathbf{S}_2\right)_z$, where the J's are proportional to the static spin susceptibility tensor of the electron gas [9–11]. The total effective interaction is a competition between in-plane $J_{XX} (= J_{YY})$, Ising J_{ZZ}, and Dzyaloshinskii-Moriya J_{DM} terms. In TMDs the Ising and DM terms are generated by the SOC; their competition has been recently discussed for bulk samples [14, 16] and flakes [30]. To calculate the effective J's in our finite sample, we take the difference of the triplet and singlet configurations of impurities in the electron gas ground state [28, 34] as

$$J^{\alpha\alpha'}_{\beta\beta',\rm eff} = \frac{E(\uparrow_\beta, \uparrow_{\beta'}) - E(\uparrow_\beta, \downarrow_{\beta'})}{2S^2}. \tag{1}$$

with $S = 1/2$ in our case. β, β' represent the spin projection (x, y, z) for magnetic impurities. For instance, $J^{d_{z^2} d_{xy}}_{XY,\rm eff}$ is the interaction strength between impurities, when the spin of the first points in the x direction and is hybridized to a d_{z^2} orbital in the lattice, and the spin of the second points along y and is hybridized to a d_{xy} orbital. This non-perturbative approach is valid

even for large values of local $\mathcal{J}$ and is capable of generating results for any separation between impurities [28]. The ground state energy of the system, including both impurities, is defined as the sum of the sorted energy states of the full Hamiltonian up to the Fermi energy $\epsilon_{\rm F}$, as $E(\mathbf{S}_1^{\rm imp}, \mathbf{S}_2^{\rm imp}) = \sum_{s=\uparrow,\downarrow} \sum_{i=1}^{\epsilon_{\rm F}} \epsilon_{i,s}$. $\epsilon_{i,s}$ are obtained by exact numerical diagonalization of the full Hamiltonian, described by a matrix of $6N_{sites} \times 6N_{sites}$.

3. Results

Our flakes have 50 rows, corresponding to a total of 1275 Mo atoms ($\approx$ 160 Å on edge). This triangular flake is shown schematically in Fig. 1. We study the RKKY interaction for p-doping levels lying inside the optical gap [see Fig. 2(b)], where ≈ 100 energy states have been brought from the bulk valence band into the gap. The midgap levels correspond to dopings from 1.82×10^{12} to 9.08×10^{13} holes/cm^2 (or from 2 to 100 holes). MoS_2 p-doping can be achieved by substituting Mo with Nb [35, 36], Mn [37, 38] or other transition metals [39].

Two magnetic impurities are connected to an edge of the flake, keeping one fixed and moving the second one along the zigzag edge, as shown in Fig. 1. We fix the first impurity at the 10th row along the side of the flake (red impurity 1 in Fig. 1), and move the second one from the 11th row onwards (orange impurity 2 in Fig. 1). We set $\mathcal{J} = 0.3$ eV, and consider both impurities to be hybridized to Mo d_{z^2} orbitals, since they are dominant on the edges [30]. Positive (negative) values of these $J^{d_{z^2}d_{z^2}}_{\beta\beta',\rm eff}$ correspond to AFM (FM) alignment between impurities.

For all midgap levels, the d_{z^2} wave function is entirely localized at the edges of the flake. Notice that energy levels fall into groups of six nearly-degenerate states, with wave function modulations along the edge, due to finite size effects. For instance, the first 6 midgap states next to the VBM [see inset of Fig. 2(b)] show 1 antinode located in the middle of the edge, while in the last 6 midgap states there are 15 antinodes with a 3-site period, distributed along the flake edge. Figures 3(a) and (b) show two RKKY interaction profiles, for Fermi levels fixed at two different p-doped midgap levels, with 82 and 22 holes, respectively. They show the typical

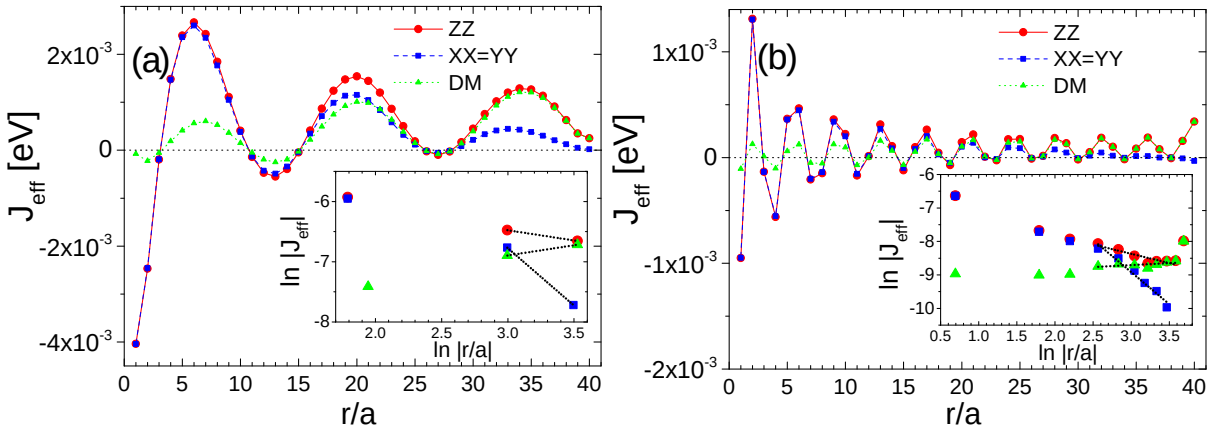

Figure 3. RKKY interaction profiles shown as $J_{\rm eff}$ vs impurity separation distance $r/$a (a is the lattice constant), for two different midgap energy levels: (a) 82 holes and (b) 22 holes. The antinode structure follows the spatial modulation of the wave function distribution on the flake edges. The insets show the logarithmic values of the maxima of each antinode, and the slopes give the decay exponent for the RKKY interacion, as shown in black-dotted lines.

RKKY behavior for all the midgap energy levels. One can observe that the three components (Ising, XX, and DM) oscillate between AFM and FM behavior, and have 3 (11) antinodes for the case of 82 (22) holes. Both the antinodes and oscillation are related to the d_{z^2} wave function distribution along the flake edge.

The Ising J_{ZZ} and in-plane interactions $J_{XX} = J_{YY}$ decay with impurity separation, but the DM component J_{DM} increases with distance. More importantly, the DM interaction is sizable and noncollinear, suggesting an effective helical ground state for multiple impurities. One can also see that the J_{XX} (J_{DM}) interaction possesses not just one decay, but another decreasing (increasing) modulation envelope attributed to size effects.

Finally we study the different spatial decay exponents. It has been shown that for Fermi levels lying on the midgap states, the decay is 1D-like (r^{-1}) or even slower ($r^{-1/2}$) [30]. We calculate this decay exponent from plots of $\ln|J_{\text{eff}}|$ vs $\ln|r/\text{a}|$ for the maxima of the J_{eff} antinodes. This is shown in dotted-black lines in the insets of Figs. 3(a) and (b). Figure 4 shows the envelope d-exponent as a function of the midgap energy levels, $J_{\text{eff}} \sim r^{d}$. For the Ising interaction is always

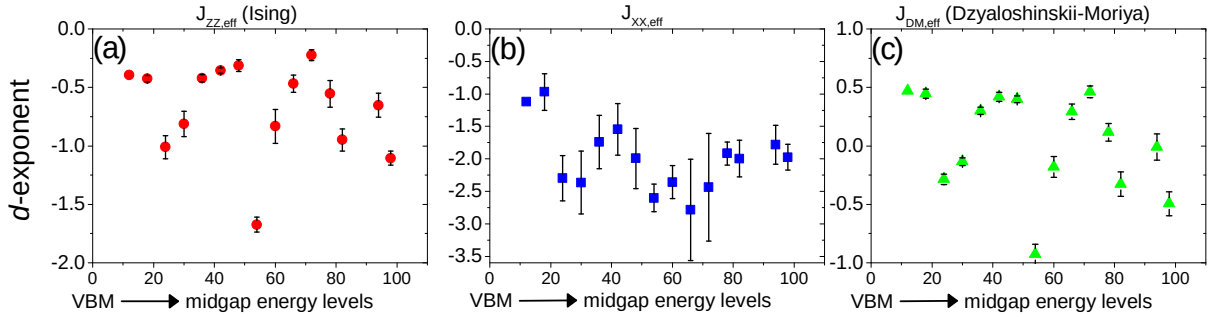

Figure 4. RKKY decay exponent d vs the sorted midgap energy levels. In the horizontal axis, zero corresponds to the VBM, and as the energy levels increase, one approaches conduction band states. Here we show the decay exponents for (a) Ising, (b) XX, and (c) Dzyaloshinskii-Moriya components. The vertical bars show the uncertainty when fitting the slopes.

negative and oscillates around $-1/2$ and -1; for the XX term, it is also negative and oscillates around -2; for DM, it oscillates around zero, ranging from $-1/2$ to $1/2$. Negative exponents are typical; a positive d represents increasing oscillation envelope with impurity separation. This sub-2D behavior of the interaction ($d<2$) suggests that the interaction is long-ranged when the impurities lie on the edges of TMDs flakes, and tunable through the impurity location and p-doping gating. Lastly, as one approaches the conduction band, the interactions become isotropic as the conduction band is not appreciably affected by the SOC.

4. Conclusions

We have studied the indirect interaction between magnetic impurities on the edges of a triangular zigzag-terminated MoS_2 flake. We focused on the role that the edge states play on the interaction between impurities. We find long ranged interactions that could be tuned via the careful deposition of magnetic impurities in locations where the wave functions are enhanced, and via selection of midgap states through doping. All midgap states localized on the edges, show sub-2D decay behavior. In particular, the DM component features positive exponents for certain states, indicating an increase of the interaction with impurity separation. This behavior is due to the existence of an envelope with a wavelength longer than the size of the flake, such that the interaction is sampling a section with positive slope. These findings could be tested with local probes, such as spin-polarized STM [40, 41].

Acknowledgments

We acknowledge support from NSF grant DMR 1508325. We thank Don Roth for help in implementing the computational calculations at Ohio University.

References

[1] Novoselov K S, Jiang D, Schedin F, Booth T J, Khotkevich V V, Morozov S V and Geim A K 2005 *Proc. Natl. Acad. Sci. U.S.A.* **102** 10451–53
[2] Geim A K and Grigorieva I V 2013 *Nature* **499** 419–25
[3] Zhu Z Y, Cheng Y C and Schwingenschlögl U 2011 *Phys. Rev.* B **84** 153402
[4] Cheiwchanchamnangij T and Lambrecht W R L 2012 *Phys. Rev.* B **85** 205302
[5] Xiao D, Liu G B, Feng W, Xu X and Yao W 2012 *Phys. Rev. Lett.* **108** 196802
[6] Mak K F, Lee C, Hone J, Shan J and Heinz T F 2010 *Phys. Rev. Lett.* **105** 136805
[7] Radisavljevic B, Radenovic A, Brivio J, Giacometti V and Kis A 2011 *Nat. Nanotechnol.* **6** 147–50
[8] Han W 2016 *APL Mater.* **4** 032401
[9] Ruderman M A and Kittel C 1954 *Phys. Rev.* **96** 99–102
[10] Kasuya T 1956 *Progr. Theor. Phys.* **16** 45–57
[11] Yosida K 1957 *Phys. Rev.* **106** 893–8
[12] Parhizgar F, Asgari R, Abedinpour S H and Zareyan M 2013 *Phys. Rev.* B **87** 125402
[13] Imamura H, Bruno P and Utsumi Y 2004 *Phys. Rev.* B **69** 121303(R)
[14] Parhizgar F, Rostami H and Asgari R 2013 *Phys. Rev.* B **87** 125401
[15] Hatami H, Kernreiter T and Zülicke U 2014 *Phys. Rev.* B **90** 045412
[16] Mastrogiuseppe D, Sandler N and Ulloa S E 2014 *Phys. Rev.* B **90** 161403(R)
[17] Chiu M H, Li M Y, Zhang W, Hsu W T, Chang W H, Terrones M, Terrones H and Li L J 2014 *ACS Nano* **8** 9649–56
[18] van der Zande A M, Huang P Y, Chenet D A, Berkelbach T C, You Y, Lee G H, Heinz T F, Reichman D R, Muller D A and Hone J C 2013 *Nat. Mater.* **12** 554–61
[19] Li Y, Zhou Z, Zhang S and Chen Z 2008 *J. Am. Chem. Soc.* **130** 16739–44
[20] Botello-Méndez A R, López-Urías F, Terrones M and Terrones H 2009 *Nanotechnology* **20** 325703
[21] Tongay S, Varnoosfaderani S S, Appleton B R, Wu J and Hebard A F 2012 *Appl. Phys. Lett.* **101** 123105
[22] Bollinger M V, Lauritsen J V, Jacobsen K W, Nørskov J K, Helveg S and Besenbacher F 2001 *Phys. Rev. Lett.* **87** 196803
[23] Zhang J, Soon J M, Loh K P, Yin J, Ding J, Sullivian M B and Wu P 2007 *Nano Lett.* **7** 2370–6
[24] Lauritsen J V, Kibsgaard J, Helveg S, Topsøe H, Clausen B S, Lægsgaard E and Besenbacher F 2007 *Nat. Nanotechnol.* **2** 53–8
[25] Xu G, Wang J, Yan B and Qi X L 2014 *Phys. Rev.* B **90** 100505(R)
[26] Chu R L, Liu G B, Yao W, Xu X, Xiao D and Zhang C 2014 *Phys. Rev.* B **89** 155317
[27] Szałowski K 2013 *J. Phys.: Condens. Matter* **25** 166001
[28] Black-Schaffer A M 2010 *Phys. Rev.* B **81** 205416
[29] Akbari-Sharbaf A and Cottam M G 2014 *J. Appl. Phys.* **116** 194309
[30] Ávalos-Ovando O, Mastrogiuseppe D and Ulloa S E 2016 *Phys. Rev.* B **93** 161404(R)
[31] Liu G B, Shan W Y, Yao Y, Yao W and Xiao D 2013 *Phys. Rev.* B **88** 085433
[32] Pavlović S and Peeters F M 2015 *Phys. Rev.* B **91** 155410
[33] Segarra C, Planelles J and Ulloa S E 2016 *Phys. Rev.* B **93** 085312
[34] Deaven D M, Rokhsar D S and Johnson M 1991 *Phys. Rev.* B **44** 5977(R)
[35] Dolui K, Rungger I, Das Pemmaraju C and Sanvito S 2013 *Phys. Rev.* B **88** 075420
[36] Laskar M R, Nath D N, Ma L, Lee E W, Lee C H, Kent T, Yang Z, Mishra R, Roldan M A, Idrobo J C, Pantelides S T, Pennycook S J, Myers R C, Wu Y and Rajan S 2014 *Appl. Phys. Lett.* **104** 092104
[37] Mishra R, Zhou W, Pennycook S J, Pantelides S T and Idrobo J C 2013 *Phys. Rev.* B **88** 144409
[38] Cong W T, Tang Z, Zhao X G and Chu J H 2015 *Sci. Rep.* **5** 9361
[39] Cheng Y C, Zhu Z Y, Mi W B, Guo Z B and Schwingenschlögl U 2013 *Phys. Rev.* B **87** 100401(R)
[40] Zhou L, Wiebe J, Lounis S, Vedmedenko E, Meier F, Blügel S, Dederichs P H and Wiesendanger R 2010 *Nat. Phys.* **6** 187–91
[41] Khajetoorians A A, Steinbrecher M, Ternes M, Bouhassoune M, dos Santos Dias M, Lounis S, Wiebe J and Wiesendanger R 2016 *Nat. Commun.* **7** 10620